JOURNAL OF AIRCRAFT
Vol. 42, No. 4, July–August 2005

Flight-Simulator Study of Airplane Encounters with Perturbed Trailing Vortices

R. E. Loucel* and J. D. Crouch†
Boeing Commercial Airplanes, Seattle, Washington 98124-2207

This study provides a preliminary, but concrete, assessment of the potential benefits of causing the breakup of airplane trailing vortices via large-scale instability, resulting in vortex rings. The 737-300 flight simulator is used to model the autopiloted response of an airplane encountering the vortices at different stages in the breakup process. A series of encounters with straight vortices is used to establish a baseline response. For the early stages of the vortex breakup, the vortices are modeled as wavy vortex filaments. For the late stages of the vortex breakup, the vortices are modeled as vortex rings, whose shape is based on experimental observation. The primary results of the study are presented in a collection of contour plots for the maximum bank angle that occurs during an encounter. The bank angles are given as a function of the horizontal and vertical vortex-intercept angles. The results show a significant reduction in the maximum bank angle, experienced by the encountering airplane, as a result of the vortex breakup. The simulations show a continuous reduction in the level of upset as the vortices become increasingly wavy and ultimately break up into rings. The most significant reductions (both in terms of the magnitudes of the upset and the likelihood of their occurrence) result from the formation of vortex rings. The results suggest that the controlled breakup of the vortices could be exploited to enable reduced airplane separations, based on a vortex-destruction concept in addition to vortex avoidance.

Nomenclature

A_v	=	wavy-vortex amplitude parameter
b	=	vortex spacing
c	=	vortex-core diameter
$\boldsymbol{r}_A$	=	position vector on airplane
$\boldsymbol{r}_v$	=	position vector on vortex
T_v	=	vortex-ring time parameter
$\boldsymbol{v}$	=	velocity vector
α	=	airplane angle of attack
β	=	airplane sideslip angle
Γ	=	vortex circulation
θ	=	wake-pitch angle
λ	=	instability wavelength
τ	=	$t/(2\pi b^2/\Gamma)$, nondimensional time
ψ	=	wake-intercept angle

Subscripts

A	=	airplane
ell	=	values based on elliptic spanload approximation
t	=	target
v	=	vortex

Introduction

Motivation

RECENT studies, aimed at reducing the required separation distances between landing aircraft, have demonstrated the potential for accelerating the breakup of airplane trailing vortices. The capacity of some airports is limited by the spacing that is imposed between in-trail airplanes on final approach during instrument meteorological conditions (IMC).[1] This spacing is imposed to ensure that the following airplane is not upset by the trailing vortices produced by the lead airplane. The imposed separations result in a reduction in capacity when compared to visual conditions. Although the current system works primarily through avoidance, breaking up the vortices could permit reduced separations between airplanes during IMC, and thus increase airport capacity.

The recent studies have exploited new instabilities and transient growth mechanisms that exist for systems of vortices with multiple vortex pairs.[2–4] These mechanisms lead to a more rapid growth than occurs on a single vortex pair.[5] Airplanes with flaps deployed produce multiple vortices in the near field, which can result in a pair of corotating vortices on each side of the aircraft farther downstream. Using conventional airplane control surfaces, Crouch et al.[6,7] demonstrated a viable scheme for breaking up the trailing vortices into vortex rings. The breakup occurs at a distance that is less than the current separation requirements. For configurations that result in a pair of counter-rotating vortices on each side of the airplane (e.g., for large horizontal-tail loading or inboard-flap retraction), there have been several studies that show rapid growth of vortex perturbations[8–11]—although, not always leading to breakup into vortex rings.

The viability of any vortex-breakup system for reducing airplane separations depends on the effectiveness in breaking up the vortices, on the impact of the system on the leading (active) airplane, and on the in situ performance of the system as measured by the following airplane. Here we focus on the system of Crouch et al.[6] The effectiveness of the system in breaking up the vortices has been demonstrated in ground-based testing and direct numerical simulations. Results show that shifting approximately 6% of the wing lift between inboard and outboard sections of the wing can break up the vortices into rings in a distance of approximately 3 nm behind a 747-400 (when scaled to flight). This distance is given as an illustration of the performance; the 747-400, or other specific configurations, was not tested. The distance required to break up the vortices depends on the details of the flap configuration, the horizontal-tail loading, and the level of forcing. Figure 1 shows a computer visualization of the vortex breakup behind a heavy airplane, flying from the upper left toward the lower right in the image. This visualization is based on scaling the towing-tank experimental results to flight.

To exploit, and optimize, a system for breaking up the vortices, the effectiveness in achieving breakup must be translated into a distance at which the vortices can be considered benign to a following

Presented as Paper 2004-1074 at the 42nd Aerospace Sciences Meeting, Reno, NV, 5–8 January 2004; received 24 February 2004; revision received 19 May 2004; accepted for publication 19 May 2004.

*Engineer; currently Systems Engineer, P.O. Box 748, Lockheed Martin Aeronautics Company—Fort Worth, MZ 1715, Fort Worth, Texas 76101.
†Technical Fellow, P.O. Box 3707, MS 67-LF.

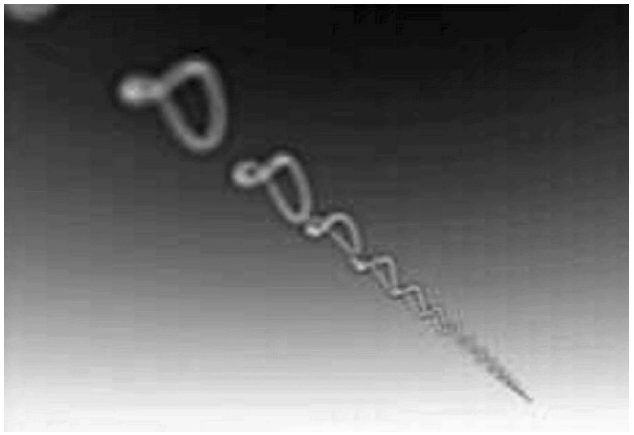

Fig. 1 Animation of trailing vortices undergoing breakup into vortex rings, after Crouch et al.[7]

airplane. The current study is an initial attempt at estimating this distance based on vortex encounters as modeled using the 737 flight simulator with an autopilot. The 737 is "flown" through the vortices at different stages in the breakup process to determine when the vortices can be considered benign. The flight-simulator results are not intended to provide an absolute measure of acceptability, but rather an indication of the relative improvement as experienced by an encountering airplane at different following distances. Any threshold for characterizing the vortex encounter as acceptable will be a strong function of the encounter altitude, a parameter not considered in the current study.

Previous Vortex-Encounter Studies

There are two basic approaches that have been used to assess the impact of trailing vortices on an encountering aircraft. The first is a static approach, where the nonuniform vortex flowfield is used to determine loads on an airplane, which is placed at different positions in the neighborhood of the vortices.[12,13] This provides an instantaneous response, or a snapshot of the vortex effects, assuming the airplane is at the prescribed location. The second approach is to use a flight simulator to consider the dynamic response of the encountering airplane (i.e., the airplane is allowed to move according the imposed loads at each time step).[14–19] This provides an integrated response to the vortices. A fairly extensive review of these methods is given by Rossow.[20]

The approach taken here is to consider the integrated response and, in particular, how this integrated response is altered by the growth of long-wavelength instabilities and post-breakup vortex rings. The basic simulator model used on the current study is the same as considered by Vasatka.[18] All of the earlier flight-simulator studies are based on straight (unperturbed) vortices. The vortices are modeled in the simulators using a strip-theory analysis; this permits the real-time calculation of the loads necessary for piloted encounters.

Piloted studies reported by Rossow[20] have shown that flight simulators provide a realistic representation of vortex encounters. The maximum bank angle is the parameter that provided the best demarcation between hazardous and nonhazardous encounters. The value of the maximum bank angle for a hazardous encounter depended on the airplane altitude.[14] Above 350 ft, an encounter was perceived to be hazardous if the maximum bank angle exceeded 10 deg, under instrument flight rules. Below 200 ft, the perceived hazard threshold was around 7 deg. The current study focuses on the maximum bank angle as a measure of the severity of an upset.

Flight-Simulator Model

The severity of a wake-vortex encounter will depend on the vortex characteristics, the height at which the encounter occurs, the orientation of the vortices relative to the flight path, the encountering-airplane response dynamics, and the response of the pilot. The primary goal of the current study is to determine the potential benefit

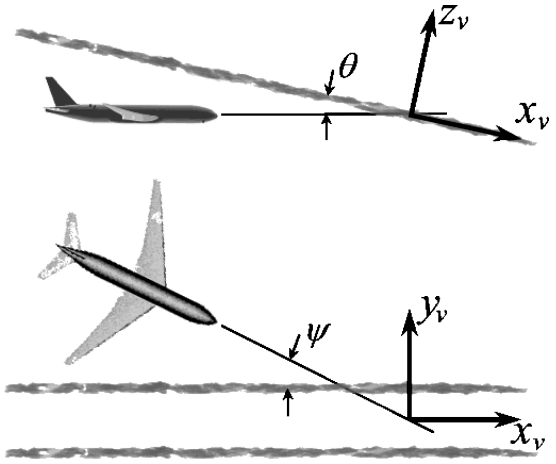

Fig. 2 Schematic showing the encountering aircraft, the trailing-vortex filaments, the vortex reference frame, the wake pitch angle relative to level flight θ, and the wake-intercept angle ψ.

of changes to the vortex characteristics that occur during the vortex-breakup process. Thus, we consider a single airplane configuration, the 737-300, to remove variations caused by the response dynamics. To remove human factors (which are acknowledged to be very significant in a real encounter), an autopilot is employed.

The effects of the vortex characteristics are determined by considering a large array of vortex encounters, covering different orientations of the vortices. The vortex orientation is described by two angles, as shown in Fig. 2. The angle θ describes the wake pitch relative to the level flight of the airplane, and the angle ψ describes the wake intercept, or grazing angle. During the encounter, the vortex flowfield is unaffected by the airplane.

Airplane Representation

The six-degree-of-freedom 737-300 simulation is built on a database for uniform-flow conditions. The effects of the vortices are modeled using a strip-theory approximation for the wings, the horizontal tail, and the vertical tail. The strips are spaced 1 ft apart, and the force on each strip is applied at the aerodynamic center. In all of the cases considered, the airplane is trimmed in level flight with landing flaps when the encounter occurs.

The basic simulator model is the same as was used in the study of Vasatka.[18] In that study, only straight vortices were considered, but both a math pilot and an autopilot were employed.

To calculate the vortex loads, the incremental vortex-induced velocity is determined at the aerodynamic center for each strip. The local vortex velocity is then added to the local airplane velocity vector at the strip. For the horizontal tail, an empirical downwash factor is applied to effectively reduce the imposed vortex velocity. The total velocity at the aerodynamic center is used to calculate the local angle of attack α and the local sideslip angle β. For the wing, the sideslip is recast as an additional α increment based on the dihedral. These angles are used to determine section lift forces from the database, which assumes uniform flow. Finally, the uniform-flow lift force is scaled using an empirical span-load function to account for some of the non-uniform-flow effects. The resulting sectional loads are integrated over the span to determine the total forces and moments.

The performance of the simulator vortex model (for straight vortices) was assessed in earlier studies using a series of test flowfields and by comparison to flight-test data.[21] Because the primary focus of the current effort is to monitor the peak bank angle, a good test case is to mimic a uniform roll rate by placing the airplane within an oversized vortex core (sized to be greater than the airplane wing span) aligned with the vortex axis. This results in a linear velocity distribution along the wing, just as if the airplane were rolling at a fixed rate. The strength of the vortex is proportional to the equivalent roll rate. The airplane loads resulting from the imposed vortex are compared to a baseline simulation with the airplane in motion

having the same roll rate in the absence of the vortices. For a 4-deg-per-second roll rate, results for the vortex model are within 2.7 and −1.5% for the two angles of attack (4 and 8 deg), which bound the nominal airplane values for the current studies. For a 10-deg-per-second roll rate, the results are within 5.2 and 0.7% for the same angles of attack.

Autopilot

The 737-300 autopilot was used to control the airplane during the encounters. This is the same autopilot that is used in the actual airplane (model SP300 used in the 737-300/400/500). The basic function of the autopilot is to provide automated control of the airplane's motion in the lateral/directional and longitudinal axes, as well as to control the flight conditions such as speed and altitude. The autopilot's capability extends from performing basic tasks such as keeping the wings level to performing complex tasks like auto land. The autopilot operates within the normal control limits of the airplane, but it does not have full control authority.

The configuration of the airplane autopilot for the wake-vortex encounter study is very basic. Only the roll and pitch modes are utilized to maintain wings level (with a limit on roll-angle excursion) and maintain a certain altitude and a particular heading.

In the roll mode, a heading-select function is used to control the airplane's heading and roll angles. This function allows the airplane to capture, or hold, a particular heading. Heading inputs range from 0 to 360 deg, by 1-deg increments. The heading value is used to set the vortex grazing angle ψ. With the heading-select function, a bank-angle limit is automatically enabled. This causes the autopilot to try and control roll-angle deviations, within the control-limit authority. The bank angle limit used for the current study is 15 deg.

The pitch mode includes altitude hold, autothrottle, and speed-select functions. The altitude hold captures and holds the target altitude, within the control-authority limits. The autothrottle allows the autopilot to control thrust levels and airplane velocity as needed to capture and/or maintain the desired altitude. With the speed-select function, the autopilot also attempts to control speed. This function is used as a backup to the altitude-hold function. Under normal conditions, the altitude hold overrides the speed select.

Vortex Flowfield Model

The flight simulator requires flowfield velocity vectors at a discrete set of points on the airplane at each time step in the simulation. The velocities are obtained from a simplified model of the trailing vortices, which are "frozen" in space and in time. This provides a good model for the flowfield experienced by a following airplane at a fixed distance to the lead airplane that produces the vortices. The model is based on theoretical and experimental results for the shape of the vortices, but the vortex details are simplified for computational efficiency within the flight simulator.

The velocity induced by a vortex filament with circulation Γ is described by the Biot–Savart law

$$\boldsymbol{v}(x_A, y_A, z_A) = \frac{\Gamma}{4\pi} \int_{L_v} \frac{(\boldsymbol{r}_v - \boldsymbol{r}_A)}{|\boldsymbol{r}_v - \boldsymbol{r}_A|^3} \times \frac{\partial \boldsymbol{r}_v}{\partial l_v}\, \mathrm{d}l_v \tag{1}$$

where $\boldsymbol{r}_v = x_v\hat{\boldsymbol{i}} + y_v\hat{\boldsymbol{j}} + z_v\hat{\boldsymbol{k}}$ is the position vector on the vortex filament of length L_v and $\boldsymbol{r}_A = x_A\hat{\boldsymbol{i}} + y_A\hat{\boldsymbol{j}} + z_A\hat{\boldsymbol{k}}$ is the position vector representing the location on the airplane where the induced velocity is calculated. The vortex position vector is time independent.

Straight Vortices

The effects of vortex distortion are measured against a baseline of encounters with straight vortex filaments. The straight vortices are modeled by a pair of counter-rotating Rankine vortices. The pair of vortices is characterized by the vortex circulation Γ, the spacing between the vortices b, and the individual vortex-core diameter c.

Using the vortex coordinate system shown in Fig. 2, the starboard vortex is given by $\Gamma_v = -\Gamma$, $x_v = x + x_A$, $y_v = +b/2$, $z_v = 0$, and the port vortex is given by $\Gamma_v = +\Gamma$, $x_v = x + x_A$, $y_v = -b/2$, $z_v = 0$, where $x \in (-\infty, \infty)$. For points outside the vortex core ($r > c/2$), the induced-velocity contribution from one of the vortices is given by

$$\boldsymbol{v}(x_A, y_A, z_A) = \frac{\Gamma_v}{4\pi} \int_{-\infty}^{\infty} \frac{(z\hat{\boldsymbol{j}} - y\hat{\boldsymbol{k}})}{r^3}\, \mathrm{d}x$$

$$= \frac{\Gamma_v}{4\pi} \frac{(zx\hat{\boldsymbol{j}} - yx\hat{\boldsymbol{k}})}{(y^2 + z^2)r} \Bigg]_{-\infty}^{\infty} \tag{2}$$

where $x = x_v - x_A$, $y = y_v - y_A$, $z = z_v - z_A$, and $r = [x^2 + y^2 + z^2]^{1/2}$. The resulting velocity field is independent of the x coordinate because the vortices are uniform in x and are assumed to extend to infinity both fore and aft of the encountering airplane. This, in conjunction with the Rankine-vortex core model, yields the well-known representation for the velocity field from a single straight-vortex filament,

$$\boldsymbol{v}(x_A, y_A, z_A) = \Gamma_v/2\pi$$

$$\begin{cases} [z/(y^2 + z^2)\hat{\boldsymbol{j}} - y/(y^2 + z^2)\hat{\boldsymbol{k}}], & \sqrt{y^2 + z^2} > c/2 \\ (4z/c^2\hat{\boldsymbol{j}} - 4y/c^2\hat{\boldsymbol{k}}), & \sqrt{y^2 + z^2} \le c/2 \end{cases} \tag{3}$$

The total vortex-induced velocity is the sum of the contributions from the starboard and port vortices.

Wavy Vortices

The wavy vortices are modeled as finite-amplitude sinusoidal perturbations to the vortex filaments. The y and z position of the vortices are displaced with a periodic dependence on x. In the vortex coordinate system of Fig. 2, the starboard vortex is given by

$$\Gamma_v = -\Gamma, \qquad x_v = x + x_A$$

$$y_v = +b/2 + A_v b\cos(\alpha x_v), \qquad z_v = +A_v b\cos(\alpha x_v)$$

and the port vortex is given by

$$\Gamma_v = +\Gamma, \qquad x_v = x + x_A$$

$$y_v = -b/2 - A_v b\cos(\alpha x_v), \qquad z_v = +A_v b\cos(\alpha x_v)$$

where $x \in (-\infty, \infty)$. The amplitude parameter A_v is used to represent different stages in the development of instabilities leading to vortex pinching, which occurs at $A_v = 0.5$. The y and z perturbations are chosen to have the same magnitude, corresponding to a 45-deg inclination of the perturbation. This is in general agreement with the instabilities known to cause breakup into vortex rings.[3–5] Other angles could be considered, but they are not expected to yield significantly different results.

The induced-velocity contribution from one of the wavy vortices is given by

$$\boldsymbol{v}(x_A, y_A, z_A) = \frac{\Gamma_v}{4\pi} \int_{-\infty}^{\infty} \frac{(yz_v' - zy_v')\hat{\boldsymbol{i}}}{r^3} + \frac{(zx_v' - xz_v')\hat{\boldsymbol{j}}}{r^3}$$

$$+ \frac{(xy_v' - yx_v')\hat{\boldsymbol{k}}}{r^3}\, \mathrm{d}x \tag{4}$$

where $x = x_v - x_A$, $y = y_v - y_A$, $z = z_v - z_A$, $r = [x^2 + y^2 + z^2]^{1/2}$, and the prime signifies $\partial/\partial x$. This integral for a wavy vortex can be solved numerically, but for large values of x it is more efficient to approximate the ends of the vortex by straight filaments. Limiting the numerical integration to N wavelengths nearest to x_A (N odd), the induced velocities from the ends of the vortices are given by straight-filament analytical expressions.

The induced velocity from one of the wavy vortices is approximated by

$$\boldsymbol{v}(x_A, y_A, z_A) = \frac{\Gamma_v}{4\pi}\int_{-N\lambda/2+\bar{x}_A}^{N\lambda/2+\bar{x}_A} \frac{(yz_v' - zy_v')\hat{\boldsymbol{i}}}{r^3} + \frac{(zx_v' - xz_v')\hat{\boldsymbol{j}}}{r^3} + \frac{(xy_v' - yx_v')\hat{\boldsymbol{k}}}{r^3}\,\mathrm{d}x + \frac{\Gamma_v}{2\pi}\left[\frac{z\hat{\boldsymbol{j}} - y\hat{\boldsymbol{k}}}{(y^2+z^2)}\right]\left(1 - \frac{N\lambda/2}{\sqrt{N^2\lambda^2/4 + y^2 + z^2}}\right) \tag{5}$$

where $\bar{x}_A = x_A - M\lambda - \lambda/2$ is the relative position of x_A within a wavelength of the vortex (e.g., at a peak, or a trough, etc.) and M is the maximum number of integer wavelengths within x_A. Over the interval $x \in (-N\lambda/2 + \bar{x}_A, N\lambda/2 + \bar{x}_A)$, the integral is evaluated numerically. Outside this interval, the straight-filament approximation is used. For a typical wavelength of $\lambda = 8b$ with $A_v = 0.4$, a value of $N = 3$ resulted in a maximum error of $0.0063\Gamma/2\pi b$ in the velocity magnitude compared to $N = 5$. The magnitude of the velocity at the location of the maximum error is $2.3\Gamma/2\pi b$, yielding a local error of less than 0.3%. The vortex encounter results are based on $N = 3$. For points (x_A, y_A, z_A) inside a vortex core, the vortex is locally approximated by a straight filament aligned with the tangent to the vortex at the minimum of r. As $A_v \to 0$, the induced velocities from the wavy vortices match the velocities given in Eq. (3).

Figure 3 shows isovelocity contours for straight vortices and wavy vortices with $A_v = 0.1$ and 0.4. The velocity magnitude for the contour corresponds to the induced velocity at the centerline of a straight vortex pair.

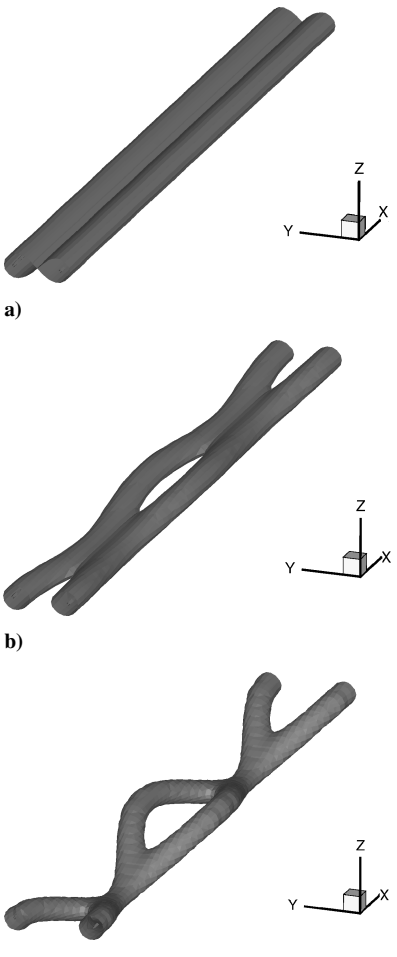

Fig. 3 Isocontours of velocity magnitude $\sqrt{(u^2+v^2+w^2)} = 4\Gamma/(2\pi b)$ for a) straight vortices and wavy vortices with b) $A_v = 0.1$ and c) $A_v = 0.4$.

Vortex Rings

The vortex rings are modeled as an infinite array of closed-loop vortex filaments. Following the vortex coordinate system of Fig. 2, the ring filaments used in this study are described by

$$\Gamma_v = +\Gamma, \qquad x_v = n\lambda + a_1\cos(s)$$

$$y_v = b_1\sin(s) + b_2\sin(3s), \qquad z_v = c_1\cos(2s) + c_2$$

with

$$a_1 = +b\left[1.3 + (\lambda/b/2.1 - 1.3)(1 - T_v)^3\right]$$

$$b_1 = -b[0.95 + (\lambda/b/2.1 - 1)\sin(\pi/5.2T_v - 0.1)]$$

$$b_2 = -b(1 - T_v)^5\sin(\pi T_v - 0.2)$$

$$c_1 = -b\cos(\pi/2T_v - \pi/6), \qquad c_2 = -b(0.4)$$

where $n = (\ldots, -2, -1, 0, 1, 2, \ldots)$ and $s \in [0, 2\pi)$. The parameter T_v is a nondimensional measure of time (or distance) beyond the point at which the vortices pinch off into rings. The vortex-ring major and minor axis switching occurs at a normalized value of $T_v = 1$, which is the maximum value for which the model was designed. A value of $T_v = 0.5$ corresponds to a distance of 3.5 wavelengths (or, for $\lambda = 8b$, 28 vortex spans) beyond the pinch point.

This simplified model (originally formulated by G.D. Miller) is based on experimental observations of vortex rings produced by active forcing of trailing-vortex instabilities taken from Crouch et al.[6] The model captures the overall shape of the rings, but the observed short-wavelength variations have been neglected. For the purpose of vortex-encounter simulations, the absence of short-wavelength variations provides a worst-case condition. The ring model provides a family of representative rings at different stages of development soon after vortex pinching. Because the model is not based on a solution of the vortex-dynamic equations, the impulse is not preserved for different values of T_v with Γ and b constant. However, for the range of conditions considered here the variation of the vertical impulse with T_v is less than 4%. This is small compared to the factor-of-10 variation in the vertical impulse for the different values of Γ and b that are considered to represent different-sized airplanes.

The velocity induced at point (x_A, y_A, z_A) by the row of vortex rings is given by

$$\boldsymbol{v}(x_A, y_A, z_A) = \sum_{n=-\infty}^{\infty}\frac{\Gamma_v}{4\pi}\int_0^{2\pi}\frac{(yz_v' - zy_v')\hat{\boldsymbol{i}}}{r^3} + \frac{(zx_v' - xz_v')\hat{\boldsymbol{j}}}{r^3} + \frac{(xy_v' - yx_v')\hat{\boldsymbol{k}}}{r^3}\,\mathrm{d}s \tag{6}$$

where $x = x_v - \bar{x}_A$, $y = y_v - y_A$, $z = z_v - z_A$, $r = [x^2 + y^2 + z^2]^{1/2}$, and the prime signifies d/ds. Also, $\bar{x}_A = x_A - M\lambda$ is the x_A position relative to the nearest vortex ring, and M is the maximum number of integer wavelengths within x_A. The variables x_v, x, and r depend on n.

Similar to the treatment for the wavy vortices, the row of vortex rings is approximated by a pair of straight filaments for large values of x. This results in a finite sum over N vortex rings (N odd), given by

$$\boldsymbol{v}(x_A, y_A, z_A) = \sum_{n=-(N-1)/2}^{(N-1)/2}\frac{\Gamma_v}{4\pi}\int_0^{2\pi}\frac{(yz_v' - zy_v')\hat{\boldsymbol{i}}}{r^3} + \frac{(zx_v' - xz_v')\hat{\boldsymbol{j}}}{r^3} + \frac{(xy_v' - yx_v')\hat{\boldsymbol{k}}}{r^3}\,\mathrm{d}s + \frac{\Gamma_v}{2\pi}\left[\frac{z\hat{\boldsymbol{j}} - y\hat{\boldsymbol{k}}}{(y^2+z^2)}\right]\left(1 - \frac{N\lambda/2}{\sqrt{N^2\lambda^2/4 + y^2 + z^2}}\right) \tag{7}$$

The vortex encounter results are based on $N = 3$ because higher values do not significantly change the induced velocities. The maximum error in the velocity magnitude is less than 1% for $T_v = 0.5$.

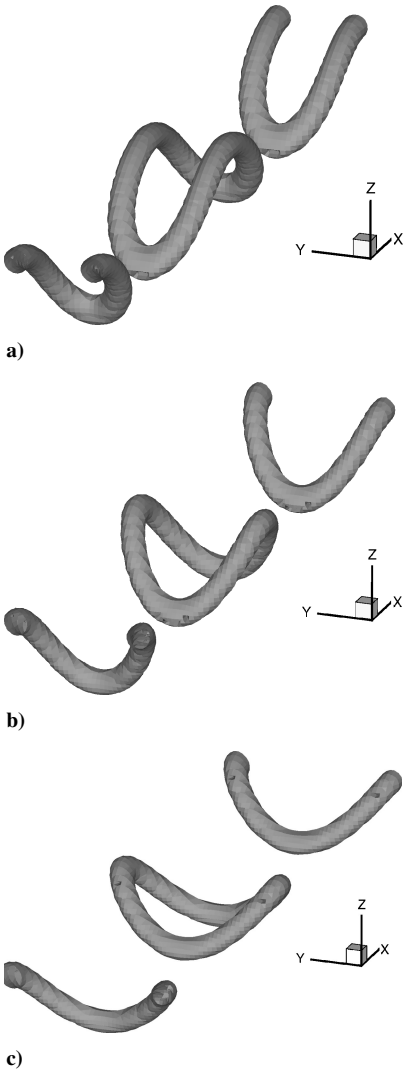

Fig. 4 Isocontours of velocity magnitude $\sqrt{(u^2+v^2+w^2)} = 4\Gamma/(2\pi b)$ for vortex rings at a) $T_v = 0.2$, b) $T_v = 0.5$, and c) $T_v = 0.8$.

For points (x_A, y_A, z_A) inside the vortex core, the vortex is locally approximated by a straight filament aligned with the tangent to the vortex at the minimum of r.

Figure 4 shows isovelocity contours for the vortex-ring flowfields with $T_v = 0.2$, 0.5, and 0.8. The velocity magnitude for the contour corresponds to the induced velocity at the centerline of a straight vortex pair, similar to Fig. 3.

Encounters with Straight Vortices

Within the 737 flight simulator, a basic vortex encounter is characterized by the vortex properties $(\Gamma, b, c/b)$ and the vortex intercept parameters (ψ, θ, x_t, z_t). The vortex strength is given by the circulation Γ, and the spanwise spacing between the vortex pair is b. The product of Γb is proportional to the weight of the airplane producing the vortices (for a given air density and airplane speed). The size of the vortices is modeled by the vortex-core diameter c. The wake-pitch angle θ and the wake-intercept angle ψ are defined in Fig. 2. The coordinates x_t and z_t correspond to the target intersection between the vortices and the encountering-airplane flight path. For straight vortices, the encounter results are independent of x_t.

Table 1 gives the vortex properties for three different-sized airplanes. The smallest circulation and vortex-span values ($\Gamma = 2500$ ft^2/s, $b = 75$ ft) correspond roughly to a 737, based on an elliptic spanload approximation. This wake provides an encounter where the lead and following airplanes are the same size. The ($\Gamma = 4000$ ft^2/s, $b = 120$ ft) case corresponds to a "heavy" airplane, and this is used as the baseline airplane in the current study. The largest values ($\Gamma = 6000$ ft^2/s, $b = 165$ ft) roughly correspond to a 747, based on an elliptic spanloading.

Table 1 Summary of wake conditions for the presented results

A/P	Γ, ft^2/s	b, ft	c/b	z_t
737	2500	75	0.1	0
767	4000	120	0.1	0
747	6000	165	0.1	0

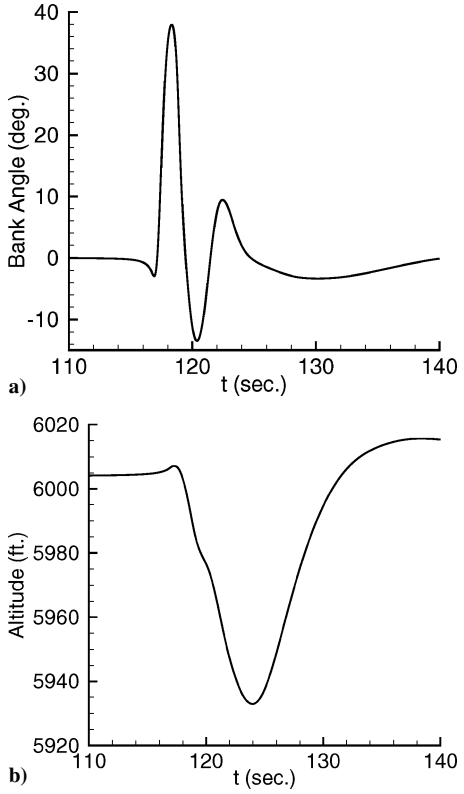

Fig. 5 Time traces of the a) bank angle and the b) altitude for a vortex encounter with wake-intercept angle $\psi = 15$ deg and wake-pitch angle $\theta = 0$ deg ($\Gamma = 4000$ ft^2/s, $b = 120$ ft, $c/b = 0.1$).

Time traces showing the bank angle and the altitude during an encounter are given in Fig. 5. These results are for the baseline vortex configuration, with $\Gamma = 4000$ ft^2/s, $b = 120$ ft, and $c/b = 0.1$. The vortex intercept parameters are $\psi = 15$ deg, $\theta = 0$ deg, and $z_t = 0$. The airplane begins to cross over the first vortex at about 117 s, and it leaves the second vortex at about 119 s. The 2-s duration of this part of the encounter is consistent with flight-test observations for an airplane with landing flaps.[15,21] The passage through the vortex pair produces the maximum bank angle of about 38 deg, which occurs just after 118 s. The secondary peaks at around 120 and 122 s are the result of the airplane trying to resume its original trajectory. The airplane drops about 25 ft as it passes through the vortex pair, but it continues to lose altitude during the remainder of the upset. In total, the airplane loses about 70 ft of altitude during the complete encounter.

Figure 6 shows the contours of the maximum bank angle for vortex encounters at different angles (ψ, θ). The contours for $\psi < 0$ (not shown) are symmetric about $\psi = 0$. Results for very small grazing angles are not realistically modeled by straight flight paths, so no results are shown for angles less than 2 deg. In practice, the small grazing angles would only occur during some form of turning maneuver. The results for very large bank angles are also not very realistic, and so the upper contour level is limited to 45 deg. In practice, a pilot would take over airplane authority well before these large bank angles would be experienced. Nonetheless, the occurrence (or nonoccurrence) of these large bank angles is an indication of the

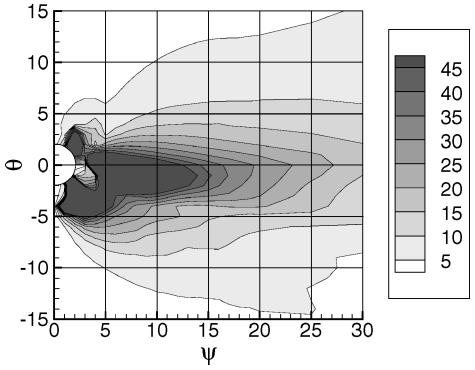

Fig. 6 Contours of maximum bank angle (deg) as a function of the wake-intercept and wake-pitch angles ($\Gamma = 4000$ ft^2/s, $b = 120$ ft, $c/b = 0.1$).

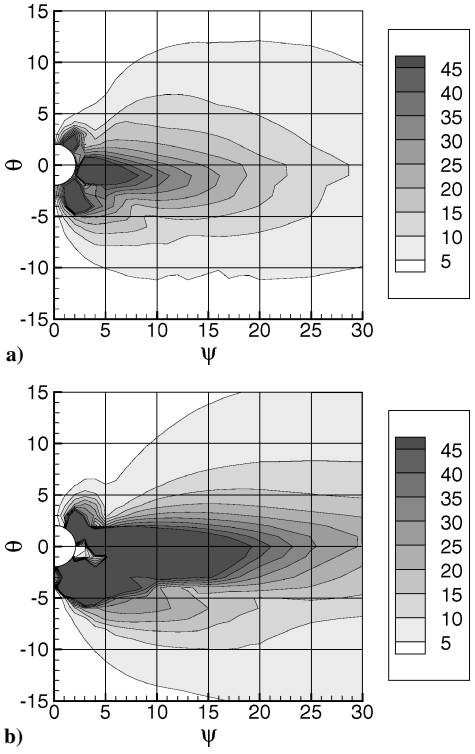

Fig. 7 Contours of maximum bank angle (deg) as a function of the wake-intercept and wake-pitch angles for different-sized leader aircraft: a) $\Gamma = 2500$ ft^2/s, $b = 75$ ft (roughly a 737); and b) $\Gamma = 6000$ ft^2/s, $b = 165$ ft (roughly a 747), ($c/b = 0.1$).

relative potential for severe upsets. Figure 6 shows that there is a very large range of encounter angles for which the maximum bank angle exceeds, say, 15 deg. This extends from roughly -5 deg $< \theta < 4$ deg and $\psi < 30$ deg.

The effect of the lead-airplane size is shown in Fig. 7, where the circulation varies by a factor of 2.4. For the smaller circulation, the range over which the bank angle exceeds 15 deg is somewhat reduced from Fig. 6, extending to roughly $\psi = 22$ deg. For the larger circulation, the 15-deg contour extends well beyond $\psi = 30$ deg, in addition to covering a wider range in θ. Not surprisingly, Fig. 7 shows that a larger airplane will produce a greater upset, and this can occur over a wider range of encounter angles.

The dominant parameter influencing the level of upset over the matrix of (ψ, θ) is the vortex circulation. For a fixed circulation level, an increase in the vortex span b resulted in a modest reduction in the level of upset. In another series of tests, bank-angle time traces showed negligible effects resulting from a 50% reduction, or a 100% increase, in the vortex-core diameter.

Encounters with Vortices Undergoing Breakup

During the breakup process, the vortices evolve from nearly straight vortices into wavy vortices and then into vortex rings. This sequence is illustrated by the velocity contours of Figs. 3 and 4. (Note these contours are not vorticity, and the left and right vortices of Fig. 3 are not touching.) Here we focus on the effect that these changes have on the maximum bank-angle contours.

Airplane encounters with wavy vortices corresponding to the baseline vortex configuration are shown in Fig. 8. The amplitudes of the waviness, $A_v = 0.1$ and 0.4, are the same levels shown in Fig. 3. A comparison of Fig. 8a with Fig. 6 shows that even a 10% waviness amplitude results in a notable reduction in the level of upset—especially for $\psi > 10$ deg. A waviness amplitude of 40% results in a very significant reduction in the maximum bank angle for almost every combination of wake-intercept and wake-pitch angle. However, there is still a small zone, $0 < \psi < 5$ deg, $-2 < \theta < -7$, where the maximum bank angles are largely unchanged. Above $\psi = 15$ deg, the maximum bank angle is less than 10 deg. The amplitude of $A_v = 0.4$ represents a large variation compared to the straight vortices, but it is still well before pinching, which occurs at $A_v = 0.5$.

The effect of the vortex waviness is similar for different-sized lead airplanes. This is shown in Fig. 9 for encounters with wavy vortices at $A_v = 0.4$. The pattern of the peak bank-angle contours is similar to the baseline case of Fig. 8. The primary effect of increasing the lead airplane size is to increase the contour values.

Results for encounters with vortex rings are given in Fig. 10 for the baseline configuration. The three nondimensional times ($T_v = 0.2$, 0.5, 0.8) correspond to distances beyond pinching of roughly 1.4, 3.5, 5.6 wavelengths, respectively. The change in response between the highly distorted wavy vortex ($A_v = 0.4$ in Fig. 8) and the early postpinch vortex rings ($T_v = 0.2$ in Fig. 10) is considerable. The vortex rings for $T_v = 0.2$ show no significant upset for larger wake-intercept angles, say, $\psi > 9$ deg; the only notable upsets occur around a few specific encounter angles $\psi = 2$ deg, $\theta = \pm 2$ deg and $\psi = 6$ deg, $\theta = \pm 4$ deg. As the value of T_v is increased, the encounter angles for notable upsets shift toward larger values of

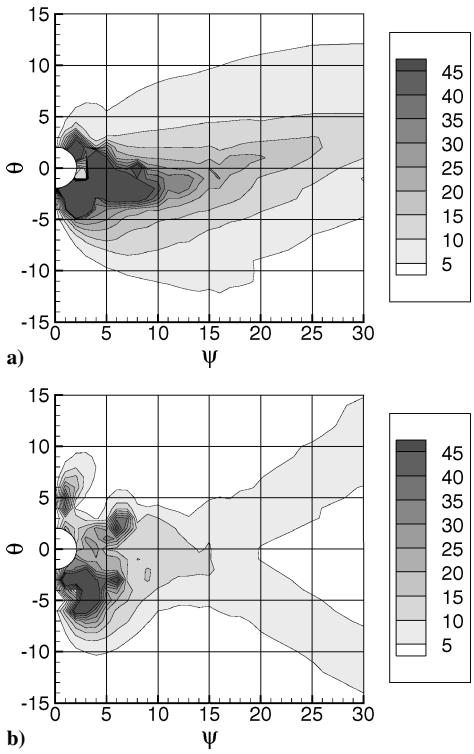

Fig. 8 Contours of maximum bank angle (deg) as a function of the wake-intercept and wake-pitch angles for wavy vortices with a) $A_v = 0.1$ and b) $A_v = 0.4$ ($\Gamma = 4000$ ft^2/s, $b = 120$ ft, $c/b = 0.1$).

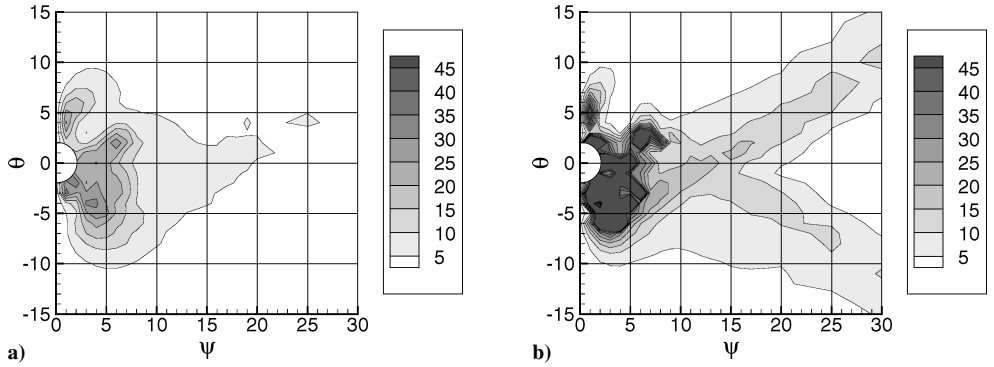

Fig. 9 Contours of maximum bank angle (deg) as a function of the wake-intercept and wake-pitch angles for wavy vortices and different-sized leader aircraft: a) $\Gamma = 2500$ ft^2/s, $b = 75$ ft (roughly a 737), and b) $\Gamma = 6000$ ft^2/s, $b = 165$ ft (roughly a 747), ($c/b = 0.1$, $A_v = 0.4$).

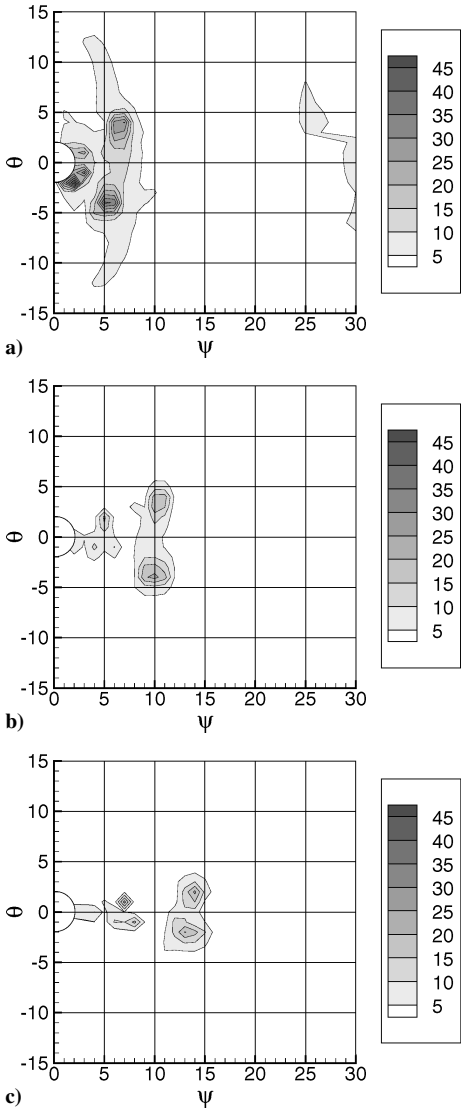

Fig. 10 Contours of maximum bank angle (deg) as a function of the wake-intercept and wake-pitch angles for vortex rings at a) $T_v = 0.2$, b) $T_v = 0.5$, and c) $T_v = 0.8$ ($\Gamma = 4000$ ft^2/s, $b = 120$ ft, $c/b = 0.1$).

ψ. For real vortices, the upset is likely to be smaller than predicted in the current study. Experiments show an additional unsteady distortion of the vortex rings, characterized by a wavelength smaller than λ. This is not accounted for in the simulator study, but it is expected to further reduce the level of upset for vortex-ring encounters.

The target intersection for the results of Fig. 10 are $x_t = 0$, $z_t = 0$. Results for $x_t = \lambda/4$, $x_t = \lambda/2$, and $z_t = \pm b/4$ all show similar results to Fig. 10. The primary effect of changing the target intersection is to shift the angles where the notable upsets occur.

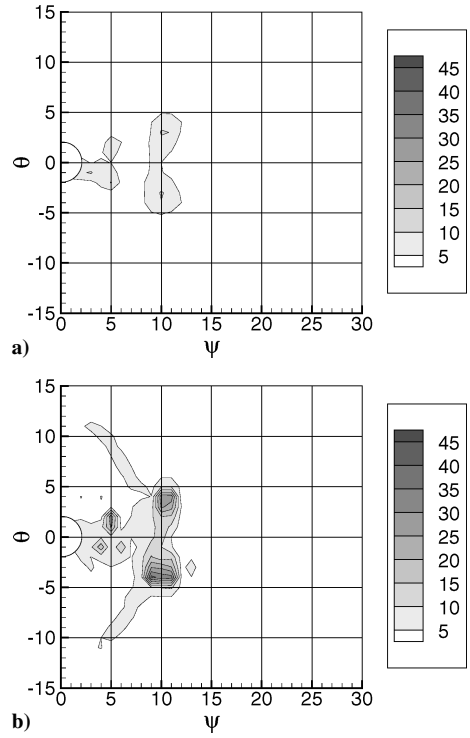

Fig. 11 Contours of maximum bank angle (deg) as a function of the wake-intercept and wake-pitch angles for vortex rings at $T_v = 0.5$ with different-sized aircraft: a) $\Gamma = 2500$ ft^2/s, $b = 75$ ft (roughly a 737), and b) $\Gamma = 6000$ ft^2/s, $b = 165$ ft, ($c/b = 0.1$).

Finally, maximum bank angles are presented in Fig. 11 for vortex rings at $T_v = 0.5$ with different-sized airplanes. For the smaller airplane, roughly the size of the encountering 737, there are only a few encounter angles that result in maximum bank angles greater than 5 deg. The maximum bank angle observed for this case is about 10 deg. This is in dramatic contrast to the straight-vortex encounters presented in Fig. 7. For the larger airplane, the contours are similar to the baseline configuration.

The active system for breakup of trailing vortices[6] leads to the formation of vortex rings at a nondimensional time of $\tau_{\text{ell}} = t\Gamma/(2\pi b^2) \approx 2.5$. For the baseline vortex configuration, this translates to a distance of approximately 2.2 n miles behind the source airplane (using an approach speed of 140 kn). The vortex-ring state characterized by $T_v = 0.5$ corresponds to a distance of 2.7 n miles behind the airplane. For a 737-sized airplane, the vortex rings form approximately 1.4 n miles behind the airplane, and $T_v = 0.5$ is approximately 1.7 n miles behind the airplane. For the 747-sized airplane, the vortex rings form at 2.9 n miles, and $T_v = 0.5$ is roughly 3.7 n miles behind the airplane.

Conclusions

This study provides a preliminary assessment of the potential benefits of controlling the breakup of airplane trailing vortices. The 737-300 flight simulator is used to model the response of an airplane encountering the vortices at different stages in the breakup process with the autopilot on. The results show a significant reduction in the maximum bank angle experienced by the encountering airplane, as a result of the vortex breakup. The simulations show a continuous reduction in the level of upset as the vortices become increasingly wavy and ultimately break up into rings. The most significant reductions (both in terms of the magnitudes of the upset and the likelihood of their occurrence) result from the formation of vortex rings.

Airplane encounters with vortex rings result in maximum bank angles of less than 5 deg for almost all of the encounter angles considered. At any given stage in the vortex-ring development, there are small zones in the wake-intercept-angle/wake-pitch-angle parameter space, where the maximum bank angles are larger than 5 deg. The peak magnitude of the maximum bank angle depends on the vortex strength. As the vortex rings age, the zones of potentially larger upsets shift toward larger wake-intercept angles. The absolute levels might not be well predicted in the current study as a result of various modeling assumptions (most significantly, the exclusive use of the autopilot), but the incremental changes should reflect the true impact of the vortex breakup. Although the current study does not provide a clear demarcation for the stage in the breakup where the vortices become benign, it does suggest that the breakup into rings is the most critical event in the process.

The results suggest two strategies leading to benign encounters with the postbreakup trailing vortices: first, when all potential upsets are removed, second, when any potential upsets are localized to an avoidable range of wake-intercept angles. The removal of all potential upsets can require that the lead airplane not be significantly larger than the encountering airplane. The acceptable relative airplane sizes will depend on the maximum bank angle that is allowed. A precise determination of this boundary will required additional study, including a better pilot model and also piloted encounters.

The localization and avoidance of any potential upset will require sufficiently aged vortices and sufficiently precise navigation and control during landing. Airplanes on final approach fly through a "tunnel in the sky" centered on the 3-deg glide slope. The tunnel is fixed by a zone around the touchdown target and expands to a larger box at the outer marker. If all airplanes stay within this tunnel, then normal limits on airplane maneuvers will yield an upper bound for the magnitude of the wake-intercept angle. The box size at the outer marker will determine the required age of the vortex rings to avoid any potential upsets.

The flight-simulator study shows a significant benefit from the breakup of the trailing vortices. In practice, airplane encounters are abnormal occurrences. Current instrument flight rules (IFR) airplane-separation requirements (from 3 to 6 miles depending on the airplane sizes) aim to avoid vortex encounters by allowing time for the vortices to descend below the flight path—well ahead of the following airplane. Under calm atmospheric conditions, the vortices are not expected to break up or decay within a 6-mile separation distance unless they are close to the ground. The current findings suggest that the vortices at 4 miles with the accelerated breakup are much more benign to an encountering airplane than natural vortices at 5 miles. Thus, an airplane that experienced an encounter would greatly benefit from the accelerated breakup of the vortices (taking the worst case for each situation). If airplane separations were reduced, the probability of having an encounter would increase; however, the breakup of the vortices could ensure that the encounters are benign. The fact that major upsets do not occur under current IFR separations, combined with the current findings, suggests that separation distances might be reduced if vortex breakup were ensured.

Acknowledgments

The authors have benefited from earlier (unpublished) work of Jim Wilborn and Harry Dellicker. We are grateful to Dave Bogue and Jim Wilborn for their guidance with the basic simulator model, to Sidney Watson for coupling the current vortex models into the 737 simulator, and to Greg Miller for providing the empirical parameterization for the vortex-ring model. Philippe Spalart, Greg Miller, and Jim Vasatka provided helpful reviews of an earlier draft of this paper.

References

[1]Robinson, J. J., "A Simulation-Based Study of the Impact of Aircraft Wake Turbulence Weight Categories on Airport Capacity," AGARD-CP-584, Neuilly-sur-Seine, France, 1996, pp. 22-1–22-15.

[2]Crouch, J. D., "Stability of Multiple Trailing-Vortex Pairs," AGARD-CP-584, Neuilly-sur-Seine, France, 1996, pp. 17-1–17-8.

[3]Crouch, J. D., "Instability and Transient Growth for Two Trailing-Vortex Pairs," *Journal of Fluid Mechanics*, Vol. 350, 1997, pp. 311–330.

[4]Fabre, D., Jacquin, L., and Loof, A., "Optimal Perturbations in a Four-Vortex Aircraft Wake in Counter-Rotating Configuration," *Journal of Fluid Mechanics*, Vol. 451, 2002, pp. 319–328.

[5]Crow, S. C., "Stability Theory for a Pair of Trailing Vortices," *AIAA Journal*, Vol. 8, No. 12, 1970, pp. 2172–2179.

[6]Crouch, J. D., Miller, G. D., and Spalart, P. R., "Active-Control System for Breakup of Airplane Trailing Vortices," *AIAA Journal*, Vol. 39, No. 12, 2001, pp. 2374–2381.

[7]Crouch, J. D., Miller, G. D., and Spalart, P. R., "Development of an Active System to Break up Trailing Vortices Behind Commercial Airplanes," *Aero Magazine*, No. 14, 2001, pp. 24–31.

[8]Quackenbush, T., Bilanin, A., Batcho, P., McKilipp, R., and Carpenter, B., "Implementation of Vortex Wake Control Using SMA-Actuated Devices," *Proceedings of the SPIE*, Vol. 3044, 1997, pp. 134–146.

[9]Rennich, S. C., and Lele, S. K., "A Method for Accelerating the Destruction of Aircraft Wake Vortices," *Journal of Aircraft*, Vol. 36, No. 12, 1999, pp. 398–404.

[10]Fabre, D., and Jacquin, L., "Stability of a Four-Vortex Aircraft Wake Model," *Physics of Fluids*, Vol. 12, No. 10, 2000, pp. 2438–2443.

[11]Ortega, J., and Savas, O., "Rapidly Growing Instability Mode in Trailing Multiple-Vortex Wakes," *AIAA Journal*, Vol. 39, 2001, pp. 750–754.

[12]Rossow, V. J., Sacco, J. N., Askins, P. A., Bisbee, L. S., and Smith, S. M., "Measurements on 80- by 120-Foot Wind Tunnel of Hazard Posed by Lift-Generated Wakes," AIAA Paper 93-3518, 1993.

[13]Holzapfel, F., Gerz, T., Frech, M., and Dornbrack, A., "Wake Vortices in Convective Boundary Layer and Their Influence on Following Aircraft," *Journal of Aircraft*, Vol. 37, No. 6, 2000, pp. 1001–1007.

[14]Sammonds, R. I., Stinnett, G. W., Jr., and Larsen, W. E., "Wake Vortex Encounter Hazard Criteria for Two Aircraft Classes," NASA TM-X73113, June 1976.

[15]Tinling, B. E., "Estimation of Vortex-Induced Roll Excursions Based on Flight and Simulator Results," *Proceedings of the Aircraft Wake Vortices Conference*, edited by J. Hallock, Report FAA-RD-77-68, 1977, pp. 11–22.

[16]Hastings, E. C., and Keyser, G. L., "Simulator Study of Vortex Encounters by a Twin-Engine, Commercial, Jet Transport Airplane," NASA TP-1966, Feb. 1982.

[17]Reimer, H. M., and Vicroy, D. D., "A Preliminary Study of Wake Vortex Encounter Hazard Boundary for a B737-100 Airplane," NASA TM-110223, April 1996.

[18]Vasatka, J., "The Dynamic Response of a Twin-Engine Commercial Jet Transport to Wake Vortex Encounters," AGARD-CP-584, Neuilly-sur-Seine, France, 1996, pp. 14-1–14-12.

[19]Hahn, K.-U., "Coping with Wake Vortex," *ICAS 2002 Congress*, pp. 732-1–732-14, 2002.

[20]Rossow, V. J., "Lift-Generated Vortex Wakes of Subsonic Transport Aircraft," *Progress in Aerospace Sciences*, Vol. 35, 1999, pp. 507–660.

[21]Wilborn, J. E., and Dellicker, H. B., "Derivation of Lateral and Directional Flight Controls Positions for the USAir 427 Accident," Boeing Coordination Sheet AERO-B-B132-C96-101, 1996.